Sensible and latent heat transfer across the air-water interface in wind-driven turbulence

S. Komori, R. Kurose, N. Takagaki, S. Ohtsubo, K. Iwano,
K. Handa and S. Shimada

*Department of Mechanical Engineering and Science, Advanced Research Institute of
Fluid Science and Engineering, Kyoto University, Kyoto 606-8501, Japan
E-mail: komori@mech.kyoto-u.ac.jp*

Abstract- Heat transfer mechanism across the sheared air-water interface was investigated through evaporation experiments in a wind-wave tank. Flow, temperature and humidity fields near the air-water interface were measured using a laser Doppler velocimetry (LDV), a particle image velocimetry (PIV), a cold film probe and an infrared hygrometer. The results show that the heat transfer coefficient on the water side increases with the free-stream wind speed and has a small plateau in the middle wind speed region where the streaky flow structure due to longitudinal vortices changes to patchy one due to breaking waves. On the air side, the sensible heat transfer coefficint monotomically inceases with the free-stream wind speed, whereas the latent heat transfer coefficient similarly has a small plateau in the middle wind speed region. These suggest that the sensible and latent heat transfer across the sheared air-water interface are dominated by turbulent organized motions in air and water flows, respectively.
Key Words: Wind wave, Air-water interface, Sensible heat transfer, Latent heat transfer, Turbulence

1. Introduction

Climate change owing to increasing release of carbon dioxide has been warningly predicted through numerical simulations based on the atmosphere-ocean general circulation model (AOGCM). In order to precisely predict such climate change and abnormal weather, it is of importance to examine some submodels used in the AOGCM without theoretical and experimental verifications. One of the uncertain submodels is the bulk model for estimating heat transfer across the air-sea interface. The bulk model gives the total heat flux per unit area Q_T on the water side by

$$Q_T = \rho_W C_{p,w} \, h_L \Delta T \,, \tag{1}$$

where ρ_W is the water density, $C_{p,w}$ the specific heat of water, h_L the heat transfer coefficient on the water side and ΔT the temperature difference between the interface and bulk water. However, ΔT is so small in oceans that precise data of ΔT cannot be available. Therefore, Q_T for the air-sea

interface is estimated on the air side by

$$Q_T = Q_H + Q_E + Q_R,\qquad(2)$$

where Q_H is the sensible heat flux, Q_E the latent heat flux and Q_R the radiative heat flux. By using temperature and specific humidity differences between atmosphere and sea surface, ΔT and Δq, together with sensible and latent heat flux transfer coefficients, C_H and C_E, the sensible and latent heat fluxes, Q_H and Q_E, are given by

$$Q_H = \rho_a C_{p,a}\, C_H U \Delta T,\qquad(3)$$

$$Q_E = \rho_a L_V\, C_E U \Delta q,\qquad(4)$$

where U is the wind speed above the air-sea interface, ρ_a the air density, $C_{p,a}$ the constant pressure specific heat of air and L_V the evaporative latent heat.

The conventional bulk models are based on the assumption that the heat flux is proportional to the wind-speed over the air-sea interface and the values of C_H and C_E in equations (3) and (4) are constant irrespective of velocity and temperature fields (Blanc, 1985; DeCosmo et al., 1996). However, the values of C_H and C_E measured in oceans are so scattered among previous studies that it is difficult to verify the assumption in the conventional bulk models. In addition, it is found that mass transfer across the sheared air-water interface is controlled by turbulent organized surface-renewal eddies in the water flow below the interface and the mass transfer coefficient is not given by a simple proportional relation with the wind-speed (Komori et al., 1982, 1993). Therefore, heat transfer should be considered to be similarly controlled by the turbulent organized surface-renewal eddies in the water flow and the relationship between heat transfer and turbulent motions should be fully investigated in wind-driven turbulence. However, the details of heat transfer have not been investigated in previous studies, since it is very difficult to precisely measure sensible, latent and radiative heat transfer in equation (2).

In order to confirm whether the conventional bulk models are applicable to the estimation of heat flux across the air-sea interface or not, we first have to precisely measure heat flux across the wavy sheared air-water interface and to clarify heat transfer mechanism together with turbulence structure near the interface. One of the best ways for getting reliable measurements is to perform laboratory experiments in a wind-wave tank where more steady flow and scalar fields than oceans are attained and turbulence quantities can be more precisely measured.

The purpose of this study is to clarify the mechanism of heat transfer across the wavy sheared air-water interface together with turbulence structure and to examine the conventional bulk models for estimating heat transfer rates across the air-sea interface.

2. Experiments

Figure 1 shows a sketch of a wind-wave tank used in this study. The wind-wave tank had a glass test section of 7 m-long, 0.3 m-wide and 0.8 m-high. The water depth in the tank was 0.5 m and the vertical height of the air flow above the air-water interface was 0.3 m. Nonlinear
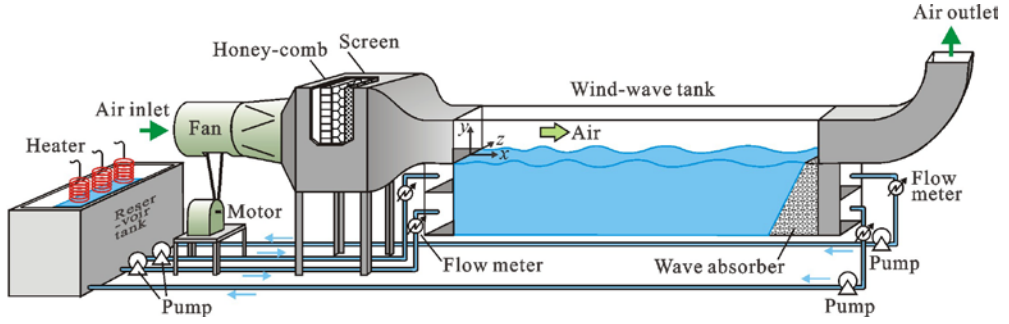
Figure 1. Experimental apparatus.

three-dimensional waves were driven in the wind-wave tank by wind. To keep the water temperature constant, water circulation system with an electric heater was employed.

To directly estimate the total heat flux Q_T, we employed the eddy correlation method, namely, Q_T was estimated by $\rho_W C_{p,w} \overline{v\theta}_{max}$, where $\overline{v\theta}_{max}$ is the maximum value of the vertical turbulent heat flux $\overline{v\theta}$ in the water flow just below the air-water interface. The instantaneous velocity and temperature at the same point were simultaneously measured using a laser Doppler velocimetry (LDV) (DANTEC 55X System) and a cold film probe (TSI 1260-10W) operated by a constant-current temperature bridge (DANTEC 55M system) in the vicinity of the surface in water flow (Nagata and Komori, 2001). Also, the temperature at the water surface T_i and the bulk temperature in water T_W were measured by a high-speed scanning infrared thermometer (NIPPON AVIONICS TVS-8502) and a thermocouple (ANRISTU-METER AM8000 series), respectively, and the temperature difference $\Delta T (= T_W - T_i)$ was estimated. The heat transfer coefficient on the water side h_L was calculated from equation (1), and the values of h_L were normalized to the heat transfer coefficient at 20 $^\circ$C by the following equation proposed by Jähne et al. (1989):

$$h_L \propto \frac{1}{\sqrt{Pr_w}}_,$$
(5)

where $Pr_w (= \nu_w / \alpha_w)$ is the Prandtl number of tap water. Here, ν_w and α_w are the dynamic viscosity and the thermal diffusivity of tap water.

Similarly, the sensible heat flux Q_H was directly estimated by the eddy correlation method, namely, Q_H was estimated by $\rho_a C_{p,a} \overline{v\theta}_{max}$, where $\overline{v\theta}_{max}$ is the maximum value of the vertical turbulent heat flux $\overline{v\theta}$ in the air flow just above the air-water interface. The instantaneous velocity and temperature at the same point were simultaneously measured using LDV (DANTEC Flow Lite LDA system) and the cold film probe, which is the same as in measurement of Q_T. Also, the water-surface temperature T_i and the bulk temperature in air T_a were measured by the same infrared thermometer and the same thermocouple used as in the measurement of Q_T, respectively. From these T_i and T_a the temperature difference $\Delta T (= T_i - T_a)$ was estimated. Air velocity was measured by a particle image velocimetry (PIV) (DANTEC Flow Map) to obtain

the vertical mean velocity profile. The wind speed at the height of 10 m above the water surface U_{10} was estimated from the logarithmic wind profile in the vicinity of the water surface. The sensible heat flux transfer coefficient C_H was calculated from equation (3), but the C_H was not normalized by the Prandtl number of air Pr_a because the changes of physical and thermal properties of air are negligibly small under present temperature condition.

On the other hand, the latent heat flux Q_E was estimated using two methods; one was a heat balance method, in which Q_E was estimated from the balance of several heat fluxes using equation (2), and the other was a water vapor balance method. In the heat balance method, the radiative heat flux Q_R in equation (2) was estimated by

$$Q_R = \varepsilon \sigma (T_i^4 - T_a^4) + Q_{R,s},\tag{6}$$

where the first term in the right hand side of equation (6) is the Stefan-Boltzmann law, ε and σ are the water-surface emissivity and the Stefan-Boltzmann constant ($= 5.67 \times 10^{-11}$), respectively. The shortwave radiative heat flux $Q_{R,s}$ was negligibly small in present laboratory experiments. Using Q_H and Q_R together with Q_T measured in the water flow, the latent heat flux Q_E was calculated from equation (2). The water vapor balance method is a similar method to the mass (CO_2) balance method for estimating the CO_2 flux across the air-water interface used in Komori et al. (1993). By taking the water vapor balance from the vertical mean vapor concentration and velocity profiles at the two stations of $x = 3$ and 5 m in the wind wave tank (see Figure 2) using an infrared hygrometer (LI-COR LI-7000) and PIV, the sensible heat flux E per unit area was estimated at $x = 4$ m from the following equation:

$$
\begin{aligned}
E &= \frac{1}{l_x}\frac{1}{2l_z}(E_5 - E_3) \\
&= \rho_a \frac{1}{l_x}\frac{1}{2l_z}\left\{ \int_{-l_z}^{l_z}\int_0^{\delta_q} U_5(y,z)\Delta q_5(y,z)dydz - \int_{-l_z}^{l_z}\int_0^{\delta_q} U_3(y,z)\Delta q_3(y,z)dydz \right\},
\end{aligned}
\tag{7}
$$

where l_x, l_z, δ_q, and q are the distance between two stations of $x = 3$ and 5 m, the half width of wind-wave tank, the thickness of the water vapor concentration boundary layer, and the water vapor concentration, respectively. Using this E, the latent heat flux Q_E is given by

$$Q_E = L_V E \ .\tag{8}$$

The latent heat flux transfer coefficient C_E was calculated from equation (4), but C_E was not normalized by the Schmidt number of water vapor in air Sc_a because the changes of the physical and thermal properties of air are negligibly small under present temperature condition.
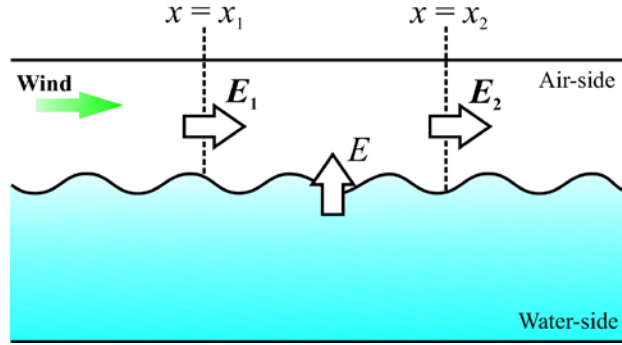
Figure 2. Measurement of H_2O flux by taking a water vapor balance on the air side.

In order to measure the latent heat flux across the breaking air-water interface in high wind speed region, a probe for sampling the water vapor in air was affected by dispersed water droplets. To overcome this problem, we horizontally lined two probes in a row and the distance between two probes was 5 mm at most. Two different hygrometers were used here for measuring the water vapor from two probes simultaneously. When one of sampling data differs from another one, we rejected the data, because this suggested that some dispersed droplets are contacting the probes.

In addition to the measurements of these heat fluxes, the frequency of the appearance of surface-renewal eddies in the water flow, f_S, was estimated by applying a VITA technique to instantaneous vertical turbulent heat flux signal (Komori et al., 1993).

The measurements of the heat fluxes (Q_T and Q_H) and f_S were carried out at $x = 4$m (fetch) from the entrance ($x = 0$m) into the test section. The mean air velocity and mean specific humidity were measured at $x = 3$ and 5m to use the water vapor balance method. The measurements were done under the free-stream wind speed of $U_\infty = 4 \sim 16.5$m/s and the air-water bulk mean temperature difference of $\Delta T = 15$K. In addition, the effect of salinity on heat transfer was investigated by comparing heat fluxes between filtered tap water and 3.5 wt% salt water.

3. Results and discussion

3.1 Heat transfer coefficient on the water side

Figure 3 shows the distribution of the heat transfer coefficient h_L on the water side againt the free-stream wind speed U_∞. The coefficient h_L increases with U_∞ and its profile has a small plateau in the middle wind speed region of $U_\infty = 7.5 \sim 10$ m/s. The similar plateau in the middle wind speed region was observed for the mass transfer coefficient k_L (Komori et al., 1993; Komori and Shimada, 1995), but the cause has not been well understood. In the figure, the values for 3.5 wt% salt water are also plotted against U_∞. Here, the values of h_L for 3.5 wt% salt water are normalized by the follwoing equation derived from equation (5):

$$h_{LF} = h_{LS}\sqrt{\frac{Pr_S}{Pr_F}} \,, \tag{9}$$
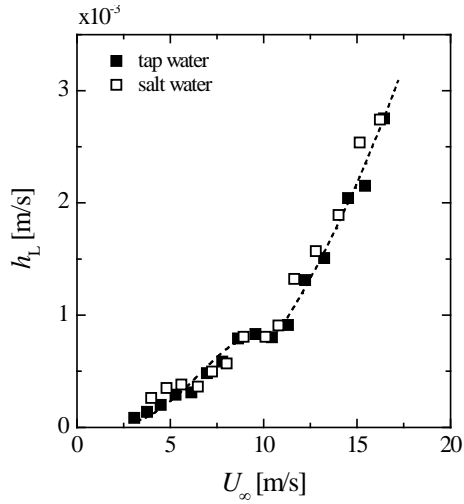
Figure 3. Heat transfer coefficient on the water side h_L againt free-stream wind speed U_∞.
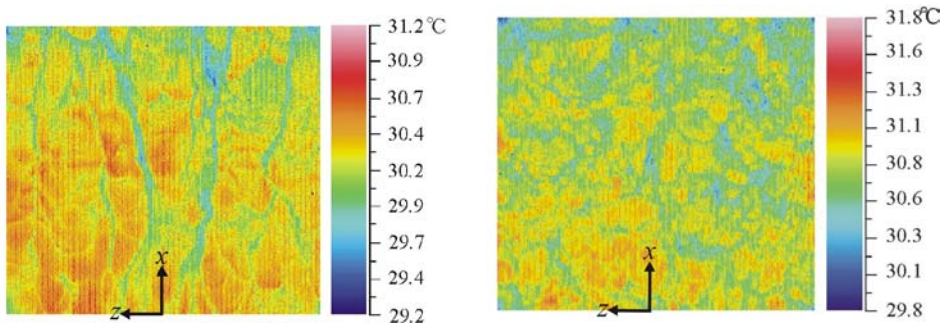
Figure 4. Instantaneous surface temperature at free-stream wind speeds of
$U_\infty = 3.1$ m/s (left hand side) and 13.2 m/s (right hand side).
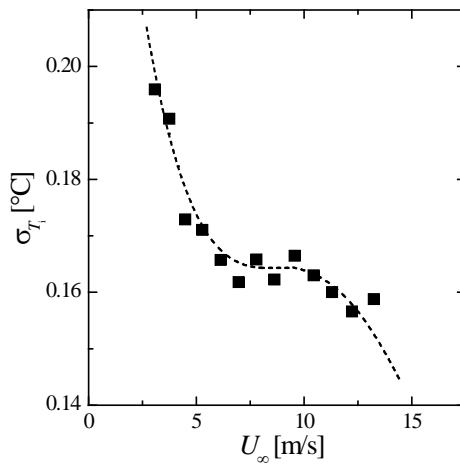
Figure 5. Standard deviation of surface temperature against free-stream wind speed U_∞.
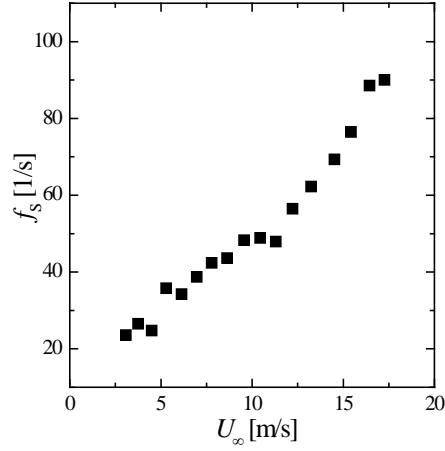
Figure 6. Frequency of the appearance of surface-renewal eddies in the water flow f_S against free-stream wind speed U_∞.

where Pr_S and Pr_F are the Prandtl numbers for salt and tap waters. There is no significant difference in h_L between tap water and 3.5 wt% salt water. This suggests that salinity does not affect on h_L.

In order to investigate the behavior of h_L against U_∞ in more detail, the surface temperature and standard deviation of surface temperature σ_T, which were measured by a high-speed scanning infrared thermometer, were compared. Figure 4 shows the surface temperature distributions at typical low and high wind speeds of $U_\infty = 3.1$ m/s and 13.2 m/s, and figure 5 shows the relationship between σ_T and U_∞. It is found that the surface temperature pattern changes from streaky structure to patchy one and σ_T decreases with increasing U_∞. Also, the profile of σ_T has a similar plateau in the middle wind speed region as shown in the profile of h_L. These suggest that the heat transfer mechanism drastically changes with the wind speed and the transition takes place in the middle wind speed region of $U_\infty = 7.5 \sim 10$ m/s. In the low wind speed region, the turbulence structure generated on the water side beneath the sheared air-water interface is found to be similar to that beneath the flat air-water interface (Tsai et al., 2005; Komori et al., 2010). Furthermore, by performing a DNS of wind-driven turbulence and scalar transfer at sheared gas-liquid interfaces, Komori et al. (2010) suggested that the scalar transfer is mainly controlled by the longitudinal vortices related to the bursting motions on the liquid side even for the wind-wave interface under the low-wind speed condition. The streaky structure in the surface temperature distribution at the low wind speed of $U_\infty = 3.1$ m/s in figure 4 supports their DNS results. That is, the longitudinal vortices are regarded as the surface-renewal eddies, which contribute to the heat transfer across the air-water interface. On the other hand, it is impossible to numerically simulate the turbulence structure at higher wind speed than 10 m/s where breaking waves actively appear. In such higher wind speed region, it is considered that the longitudinal vortices related to the bursting motions are disturbed by the breaking waves
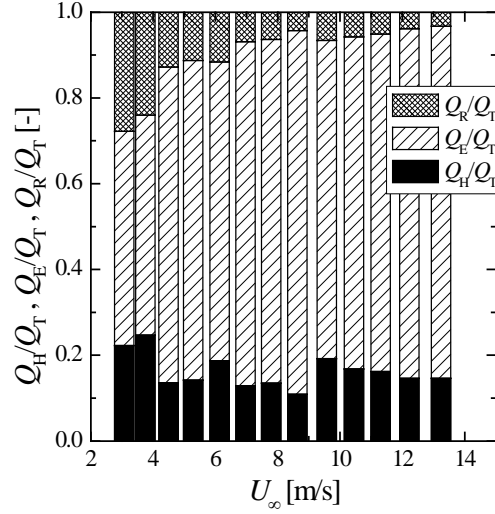
Figure 7. Ratios of heat fluxes to the total flux versus free-stream wind-speed U_∞.

and therefore the patchy structure is formed.

The reason why both h_L and σ_T have the plateaus in the middle wind speed region of $U_\infty = 7.5 \sim 10$ m/s may be given by the relation between friction drag and pressure drag acting on the air-water interface. That is, although the form drag (pressure drag) increases with growing waves, the increase in the friction drag becomes suppressed by the appearance of the flow separation behind the crests of the growing waves in the middle wind speed region. In fact, the frequency of the appearance of surface-renewal eddies in the water flow, f_S, which was estimated by applying a VITA technique to instantaneous vertical heat flux $v\theta$, has a similar trend to h_L as shown in figure 6.

3.2 Sensible and latent heat transfer coefficients on the air side

The ratios of sensible, latent, and radiative heat fluxes (Q_H, Q_E, and Q_R) to the total heat flux Q_T across the wavy sheared air-water interface against the free-stream wind speed U_∞ are shown in figure 7. It is evident that the latent heat flux dominates the heat transfer across the air-water interface on the air side in present laboratory experiments.

Figure 8 shows the distributions of sensible and latent heat flux transfer coefficients C_H and C_E obtained by substituting the above sensible and latent heat fluxes Q_H and Q_E into equations (3) and (4) against the wind speed at the height of 10 m above the water surface U_{10}, together with the best-fit curves of previous field measuements. It is found that the sensible heat flux transfer coefficient C_H is almost constant irrespective of the wind speed, but it is smaller than the field measurements. On the other hand, C_E shows the complicated dependence of wind speed and differs from the field measurements. This suggests that the conventional assumption for the same constant value around unity for C_H and C_E is not suitable for estimating the heat flux on the air side. Instead of such transfer coefficients, we propose the following sensible and latent heat transfer coefficients h_A and k_A:
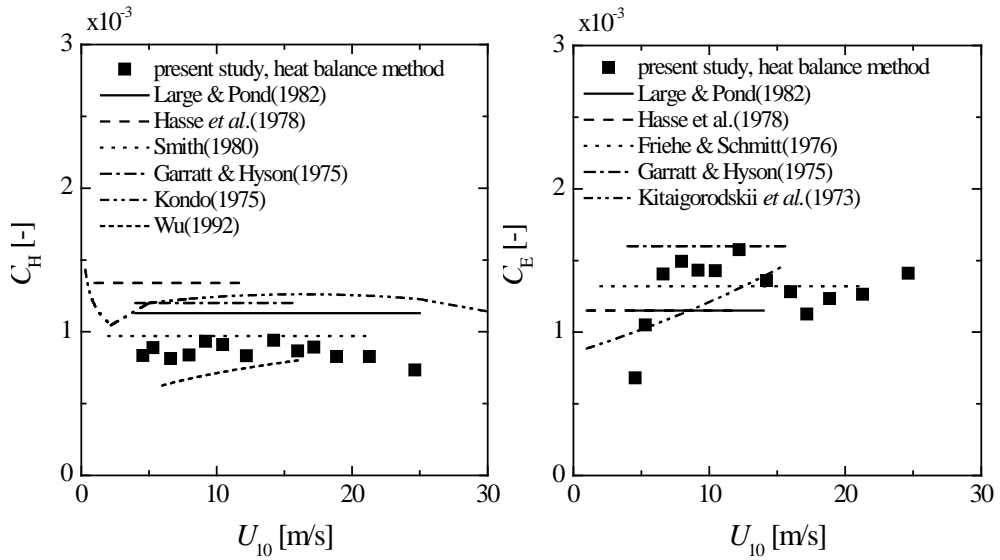
Figure 8. Sensible and latent heat flux transfer coefficients C_H and C_E against wind speed U_{10}.
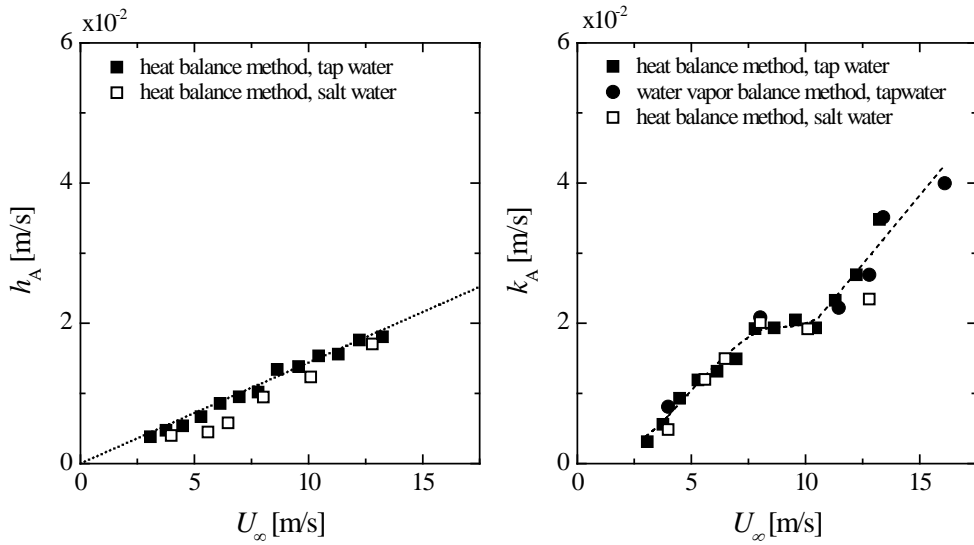
Figure 9. Relationship between sensible and latent heat transfer coefficients h_A and k_A and free-stream wind speed U_∞.

$$Q_H = \rho_a C_{p,a} h_A \Delta T \, , \tag{10}$$

$$Q_E = \rho_a L_V \, k_A \Delta q \, , \tag{11}$$

where ΔT and Δq are the temperature and humidty differences between the bulk air flow and the interface. Figure 9 shows the distributions of h_A and k_A against the free-stream wind speed U_∞. The coefficient h_A is proportional to U_∞, and k_A shows very similar behavior to the heat transfer coefficient on the water side h_L in figure 3. This suggests that sensible heat transfer is controlled by the air turbulence, whereas the latent heat transfer is controlled by the water turbulence. Figure 7 also suggests that the latent heat transfer governs the total heat transfer across the wavy sheared air-water interface.

To confirm the reliability of the heat balance method, we also estimated Q_E using equations (7) and (8), which is named as the water vapor balance method. The values of k_A estimated from the water vapor balance method are added in figure 9. The values calculated from both the heat balance method and water vapor balance method well correspond with each other. This suggests that k_A is measured with high accuracy.

The values of the heat transfer coefficients h_A and k_A for 3.5 wt% salt water are plotted against U_∞ in figure 9 as well as h_L in figure 3. There is no significant difference between tap water and 3.5 wt% salt water. This fact together with h_L in figure 3 suggests that salinity does not affect heat transfer across air-water interface.

4. Conclusions

Heat transfer mechanism across the sheared air-water interface was investigated through evaporation experiments in a wind-wave tank. The main results obtained from this study can be summarized as follows.

(1) The heat transfer coefficient on the water side increases with the free-stream wind speed and has a small plateau in the middle wind speed region where the streaky flow structure changes to patchy one.

(2) Instead of the conventional sensible and latent heat flux transfer coefficients on the air side, new heat transfer coefficients are proposed. The proposed sensible heat transfer coefficient monotomically inceases with the free-stream wind speed. On the other hand, similar to the heat transfer coefficient on the water side, the proposed latent heat transfer coefficient on the air side has a small plateau in the middle wind speed region. These suggest that the sensible and latent heat transfer across the sheared air-water interface are dominated by turbulent motions in the water and air flows, respectively.

(3) Effects of water salinity on heat transfer across the wavy sheared air-water interface are negligibly small.

References

Blanc, T. V., (1985), Variation of bulk-derived surface flux, stability, and roughness results due to the use of different transfer coefficient schemes, *J. Phys. Oceanogr.*, *15*, 650-669.

DeCosmo, J., K. B. Katsaros, S. D. Smith, R. J. Anderson, W. A. Oost, K. Bumke, and H. Chadwick (1996), Air-sea exchange of water vapor and sensible heat: The Humudity Exchange Over the Sea (HEXOS) results, *J. Geophys. Res.*, *101*, 12001–12016.

Friehe, C. A., and K. F. Schmitt, (1976), Parameterization of air-sea interface fluxes of sensible heat and moisture by the bulk aerodynamic formulas, *J. Phys. Oceanogr.*, *6*, 801-809.

Garratt J. R. and P. Hyson, (1975), Vertical fluxes of momentum sensible heat and water vapour during theair mass transformation experiment (AMTEX) 1974, *J. Meteorol. Soc. Japan.*, *53*(2), 149-160.

Hasse, L., M. Grunewald, J. Wucknitz, M. Dunckel, and D. Schriever (1978), Profile derived turbulent fluxes in the surface layer under disturbed and undisturbed conditions during GATE, *Meteor Forschungsergeb*, *13*, 24-40.

Jähne, B., P. Libner, R. Fischer, T. Billen, and J. Plate (1989), Investigating the transfer processes across the free aqueous viscous boundary layer by the controlled flux method, *Tellus*, *92*, 177-195.

Kitaigorodskii, S. A., A. Kuznetsov, and G. N. Panin (1973), Coefficients of drag, sensible heat, and evaporation in the atmosphere over the surface of the sea, *Izv. Acad. Sci. USSR, Atmos. Ocean. Phys.*, *9*, 644-647.

Komori S., H. Ueda, F. Ogino, T. Mizushina (1982), Turbulence Structure and Transport Mechanism at the Free Surface in an Open Channel Flow, *Int. J. Heat and Mass Transfer*, *25*(4), 513-521.

Komori, S., R. Nagaosa, and Y. Murakami (1993), Turbulence structure and mass transfer across a sheared air-water interface in wind-driven turbulence, *J. Fluid Mech.*, *249*, 161–183.

Komori S., and T. Shimada (1995), Gas Transfer Across a Wind-Driven Air-Water Interface and the Effects of Sea Water on CO_2 Transfer, *Air-Water Gas Transfer* (Eds. B. Jähne, and E. Monahan), AEON Verlag, 553-569.

Komori S., R. Kurose, S. Ohstubo, K. Tanno and N. Suzuki (2009), Heat and mass transfer across the wavy sheared interface in wind-driven turbulence, *Proceedings of The Sixth International Symposium on Turbulence and Shear Flow Phenomena*, (Eds. N. Kasagi, J.K. Eaton, R. Friedrich, J.A.C. Humphrey, A.V. Johansson and H.J. Sung), Seoul National University, Seoul, Korea, 399–407.

Komori, S., R. Kurose, K. Iwano, T. Ukai, N. Suzuki (2010), Direct numerical simulation of wind-driven turbulence and scalar transfer at sheared gas-liquid interfaces, *Journal of Turbulence*, *11*, 1-20.

Kondo, J. (1975), Air-sea bulk transfer coefficients in diabatic conditons. *Boundary-Layer Meteorol.*, *9*, 91-112.

Large, W. G., and S. Pond (1982), Sensible and latent heat flux measurements over the ocean, *J. Phys. Oceanogr.*, *12*, 464-482.

Nagata, K., and S. Komori (2001), Difference in Turbulent Diffusion between Active and Passive Scalars in Stable Thermal Stratification, *J. Fluid Mech.*, *430*, 361-380.

Smith, S. D. (1980), Wind Stress and Heat Flux Over the Ocean in Gale Force Winds, *J. Phys. Oceanogr.*, *10*,

709-726.

Tsai, W.-T., S.-M. Chen, and C.-H. Moeng (2005), A numerical study on the evolution and structure of a stress-driven free-surface turbulent shear flow. *J. Fluid Mech., 545*, 163-192.

Wu J., (1980), Wind-stress coefficients over sea surface near neutral conditions-a revisit,, *J. Phys. Oceanogr.*, *10*, 727-740.

Wu J., (1992), Variation of the heat transfer coefficient with environmental parameters, *J. Phys. Oceanogr.*, 22, 293-300.